Structural Characterization of CeO_2-ZrO_2/TiO_2 and $V_2O_5/CeO_2-ZrO_2/TiO_2$ Mixed Oxide Catalysts by XRD, Raman Spectroscopy, HREM, and Other Techniques

Benjaram M. Reddy,* Pandian Lakshmanan, and Ataullah Khan

Inorganic and Physical Chemistry Division, Indian Institute of Chemical Technology, Hyderabad - 500 007, India

Carlos López-Cartes,* Teresa C. Rojas, and Asunción Fernández

Instituto de Ciencia de Materiales de Sevilla (CSIC-UNSE), Avda. Américo Vespucio s/n, 41092 Sevilla, Spain

Received: September 21, 2004; In Final Form: November 16, 2004

Structural characteristics of CeO_2-ZrO_2/TiO_2 (CZ/T) and $V_2O_5/CeO_2-ZrO_2/TiO_2$ (V/CZ/T) mixed oxide catalysts have been investigated using X-ray diffraction (XRD), BET surface area, Raman spectroscopy (RS), and high-resolution transmission electron microscopy (HREM) techniques. The CeO_2-ZrO_2 (1:1 mole ratio) solid solution was deposited over a finely powdered TiO_2 support by a deposition precipitation method. A nominal 5 wt % V_2O_5 was impregnated over the calcined (773 K) CZ/T mixed oxide carrier by a wet impregnation technique. The obtained CZ/T and V/CZ/T samples were further subjected to thermal treatments from 773 to 1073 K to understand the dispersion and temperature stability of these materials. In the case of CZ/T samples, the XRD results suggest the formation of different cubic and tetragonal Ce−Zr-oxide phases, $Ce_{0.75}Zr_{0.25}O_2$, $Ce_{0.6}Zr_{0.4}O_2$, $Ce_{0.5}Zr_{0.5}O_2$, and $Ce_{0.16}Zr_{0.84}O_2$ in varying proportions depending on the treatment temperature. With increasing calcination temperature from 773 to 1073 K, the intensity of the lines pertaining to cubic $Ce_{0.6}Zr_{0.4}O_2$ and $Ce_{0.5}Zr_{0.5}O_2$ phases increased at the expense of cubic $Ce_{0.75}Zr_{0.25}O_2$, indicating more incorporation of zirconia into the ceria lattice. The TiO_2 was mainly in the anatase form whose crystallite size also increased with increasing treatment temperature. A better crystallization and more incorporation of zirconia into the ceria lattice was noted when CZ/T was impregnated with V_2O_5. However, no crystalline V_2O_5 could be seen from both XRD and RS measurements. In particular, a preferential formation of $CeVO_4$ compound and an intense tetragonal $Ce_{0.16}Zr_{0.84}O_2$ phase were noted beyond 873 K. The HREM results indicate, in the case of CZ/T samples, a well-dispersed Ce−Zr-oxide of the size ∼5 nm over the bigger crystals (∼40 nm) of TiO_2 when treated at 873 K. The exact structural features of these crystals as determined by digital diffraction analysis of experimental images reveal that the Ce−Zr-oxides are mainly in the cubic fluorite geometry and the TiO_2 is in anatase form. A better crystallization of Ce−Zr-oxides (∼8 nm) over the surface of bigger crystals of TiO_2 was noted at 1073 K. A further enhancement in the crystallite size and zirconia-rich tetragonal phase was noted in the case of V/CZ/T samples. Further, the structure of $CeVO_4$ formed was also clearly identified in conformity with XRD and RS results.

Introduction

Oxide materials containing ceria (CeO_2) have been the subject of numerous investigations in recent years because of their wide range of applications in catalysis and materials science.[1,2] The redox and catalytic properties of CeO_2 are profoundly enhanced when used in combination with other transition metal or rare earth oxides.[3] Among various elements, the introduction of zirconium into the ceria lattice has been particularly effective in the enhancement of the overall performance of CeO_2.[1−4] In fact, ceria−zirconia mixed oxides have been regarded as potential substitutes for ceria in the formulation of new generation three-way catalysts (TWC) on the basis of their superior catalytic properties resulting from the combination of oxygen storage characteristics of ceria and superior refractory properties of zirconia.[5] The ceria−zirconia mixed oxides exhibit several advantages over pure ceria, which include high thermal resistance,[6] improved reduction efficiency of the Ce^{4+}/Ce^{3+} redox couple,[7] and excellent oxygen storage/release capacity (OSC).[8−10]

Other significant applications of ceria-based materials apart from TWC include fuel cell processes, oxygen permeation membrane systems, deNO_x catalysis, exhaust combustion catalysts, and catalytic wet oxidation.[11−15] Mainly ceria-based noble metals are employed for various catalytic applications because of their increased reactivity.[3,8,16] Nevertheless, ceria-based transition metal oxides are the best option because these are much cheaper than noble metals, allowing a higher catalyst load which can compensate for the reduced reactivity. However, such approaches are very limited in the literature to the best of our knowledge.

Reactions catalyzed by supported (mostly TiO_2) vanadium oxides are numerous, including oxidative dehydrogenation of alkanes,[17,18] direct conversion of methane to aromatics,[19] selective catalytic reduction of NO_x with NH_3,[20−22] and oxidation and ammoxidation of various hydrocarbons.[23,24] In particular, oxidation catalysts are receiving a great deal of attention recently because of their major role both in the production of chemicals

* Corresponding authors. E-mail: bmreddy@iict.res.in; clopez@icmse.csic.es.

10.1021/jp045723+ CCC: $30.25
Published on Web 01/14/2005

required by selective oxidation and in the destruction of undesired products by total oxidation. Most importantly, the nature of support plays a huge influence on the physicochemical and catalytic properties of the V_2O_5 catalysts. Recent investigations reveal that $V_2O_5-CeO_2$ combination catalysts exhibit good catalytic activity for oxidative conversion of propane to propylene and ethylene,[25,26] partial oxidation of methanol to formaldehyde,[27,28] preferential oxidation of CO to CO_2, and others.[29,30] These catalysts also perform extraneous redox reactions for both selective and nonselective oxidations, the latter having extensive applications in the field of environmental catalysis for the oxidative removal of volatile organic compounds (VOCs) and other noxious emissions. As a consequence, considerable attention has been focused on the preparation, characterization, and evaluation of vanadium oxide catalysts on various supports for distinct applications.[31]

Motivated by the unique and favorable characteristics of ceria- and vanadia-based mixed oxides for various catalytic applications as discussed above,[25−31] the present systematic investigation was undertaken. In this study, the nanostructural evolution of CeO_2-ZrO_2 solid solutions over the surface of TiO_2 support and the role of dispersed vanadium oxide on this ternary oxide material was investigated. The CeO_2-ZrO_2/TiO_2 was obtained by a deposition precipitation method, and a nominal 5 wt % V_2O_5 was impregnated over the calcined (773 K) mixed oxide support. The resulting samples were further subjected to various thermal treatments from 773 to 1073 K and were examined by means of X-ray diffraction (XRD), Raman spectroscopy (RS), high-resolution transmission microscopy (HREM), and other techniques.

Experimental Section

Preparation of Samples. The CeO_2-ZrO_2 solid solution over the TiO_2 support (1:1:2 mole ratio based on oxides) was prepared by a deposition precipitation method with dilute ammonium hydroxide as hydrolyzing agent. In a typical experiment, appropriate quantities of ammonium cerium(IV) nitrate (Loba Chemie, GR grade) and zirconium(IV) nitrate (Fluka, AR grade) were dissolved separately in distilled water and mixed together. To this mixture solution, the desired quantity of finely powdered titania (EU Consortium, SA 49 m^2 g^{-1}, anatase) was added and stirred for few minutes. Dilute aqueous ammonia solution was added dropwise with vigorous stirring until the precipitation was complete. The resulting precipitate was filtered off, washed several times with distilled water, oven dried at 383 K for 12 h, and calcined at 773 K for 5 h in air atmosphere. Portions of the obtained material were once again heated at 873, 973, and 1073 K for 5 h in a closed muffle furnace in air atmosphere.

The $V_2O_5/CeO_2-ZrO_2/TiO_2$ sample was prepared by a wet impregnation method. To impregnate a nominal 5 wt % V_2O_5, the required quantity of ammonium metavanadate (Fluka, AR grade) was dissolved in aqueous oxalic acid solution (1 M), and finely powdered calcined CeO_2-ZrO_2/TiO_2 (773 K) was added. The excess water was evaporated on a water bath, and the resulting material was oven dried at 393 K for 12 h and subsequently calcined at 773 K for 5 h in a closed electrical furnace in oxygen atmosphere. Some portions of the finished sample were once again heated at 873, 973, and 1073 K for 5 h in air atmosphere.

Characterization of Samples. X-ray powder diffraction patterns have been recorded on a Siemens D 500 diffractometer using Ni-filtered Cu Kα (0.15418 nm) radiation. The intensity data were collected over a 2θ range of 3−80°, with a 0.02° step size and using a counting time of 1 s per point. The XRD phases were identified by comparison with the reference data from International Center for Diffraction Data (ICDD) files. The average crystallite size was determined with the help of the Debye−Scherrer equation using XRD data of the (111) reflection of the cubic Ce−Zr oxide and the (101) reflection of TiO_2−anatase.[32]

TABLE 1: BET Surface Area and Crystallite Size (from XRD Measurements) of CeO_2-ZrO_2/TiO_2 and $V_2O_5/CeO_2-ZrO_2/TiO_2$ Samples Calcined at Different Temperatures

sample	BET SA (m^2 g^{-1} cat)	V_2O_5 surface coverage[a]	crystallite size[b] (nm)	
			$CeZrO_x$	TiO_2 (A)
	773 K			
CeO_2-ZrO_2/TiO_2	105		3.7	20.8
5% $V_2O_5/CeO_2-ZrO_2/TiO_2$	85	0.33	4.0	22.6
	873 K			
CeO_2-ZrO_2/TiO_2	91		4.1	21.4
5% $V_2O_5/CeO_2-ZrO_2/TiO_2$	70	0.38	4.2	23.3
	973 K			
CeO_2-ZrO_2/TiO_2	69		4.6	22.0
5% $V_2O_5/CeO_2-ZrO_2/TiO_2$	49	0.50	5.4	25.5
	1073 K			
CeO_2-ZrO_2/TiO_2	52		5.0	24.8
5% $V_2O_5/CeO_2-ZrO_2/TiO_2$	30	0.66	7.8	34.6

[a] Theoretical surface coverage of vanadia over CZ/T estimated from the specific surface area of the support (ref 33). [b] The (111) peak of cubic $Ce_xZr_{1-x}O_2$ and (101) of TiO_2−anatase were used for crystallite size measurements.

The Raman spectra were recorded on a DILOR XY spectrometer equipped with a liquid-nitrogen cooled charge-coupled device (CCD) detector. The emission line at 514.5 nm from Ar^+ ion laser (Spectra Physics) was focused on the sample under microscope, the width of the analyzed spot being ~1 μm. The power of the incident beam on the sample was 3 mW. The time of acquisition was adjusted according to the intensity of the Raman scattering. The wavenumber values reported from the spectra are accurate to within 2 cm^{-1}. For each sample, the spectra were recorded at several points to ascertain the homogeneity of the sample, and the average of all of these spectra were plotted in the figures presented in this study.

The high-resolution electron microscopy studies were made on a Philips CM200 electron microscope with 0.23 nm point-to-point resolution. For electron microscopy studies, a suspension of the sample in ethanol was placed in an ultrasound bath, and then a drop of it was supported on a holey carbon grid. Once the solvent was evaporated, particles that stay on the borders of the holes in the carbon film were studied.

The specific surface area of the samples was estimated on a Micromeritics Gemini 2360 Instrument by N_2 physisorption at liquid nitrogen temperature. Before measurements, the samples were oven-dried at 393 K for 12 h and flushed in-situ with He gas for 2 h.

Results and Discussion

The N_2 BET surface areas of CeO_2-ZrO_2/TiO_2 (CZ/T) and $V_2O_5/CeO_2-ZrO_2/TiO_2$ (V/CZ/T) samples calcined at various temperatures are presented in Table 1. The CZ/T sample calcined at 773 K exhibited a specific surface area of 105 m^2 g^{-1}. A steady decrease from 105 to 52 m^2 g^{-1} has been observed (50% loss) with increasing calcination temperature from 773 to 1073 K due to sintering of the samples at higher calcination temperatures. The 5% V/CZ/T sample calcined at 773 K exhibited a surface area of 85 m^2 g^{-1}. A substantial decrease

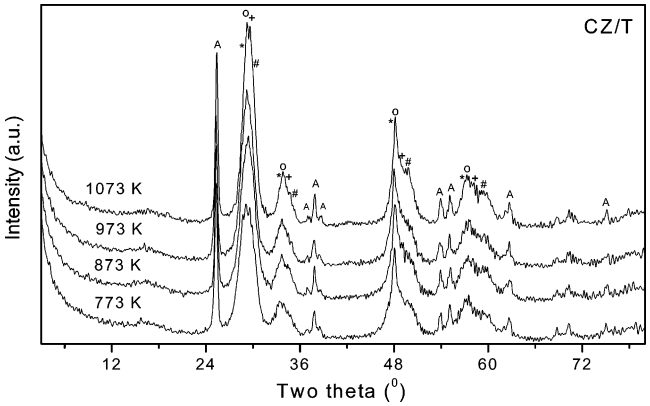

Figure 1. Powder X-ray diffraction (XRD) patterns of various CeO_2-ZrO_2/TiO_2 samples calcined at different temperatures. Peak legend is as follows: (*) lines due to $CeO_{0.75}ZrO_{0.25}$, (○) lines due to $Ce_{0.6}Zr_{0.4}O_2$, (+) lines due to $Ce_{0.5}Zr_{0.5}O_2$, (#) lines due to $Ce_{0.16}Zr_{0.84}O_2$, and (A) lines due to TiO_2−anatase.

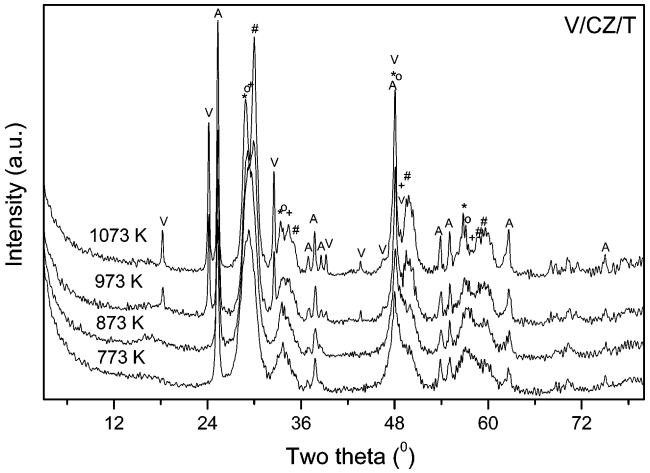

Figure 2. Powder X-ray diffraction (XRD) patterns of various $V_2O_5/CeO_2-ZrO_2/TiO_2$ samples calcined at different temperatures. Peak legend is as follows: (*) lines due to $CeO_{0.75}ZrO_{0.25}$, (○) lines due to $Ce_{0.6}Zr_{0.4}O_2$, (+) lines due to $Ce_{0.5}Zr_{0.5}O_2$, (#) lines due to $Ce_{0.16}Zr_{0.84}O_2$, (A) lines due to TiO_2−anatase, and (V) lines due to $CeVO_4$.

(65% loss) in the surface area can be noted with increasing calcination temperature. The decrease in the surface area could be due to various factors such as penetration of the dispersed vanadium oxide into the pores of the support, thereby narrowing its pore diameter, blocking some of the pores, and solid-state reactions between the dispersed vanadium oxide and the support.[33,34] The XRD measurements described in the subsequent paragraphs strongly support the latter possibility. It is a known fact in the literature that high-temperature treatment normally leads to sintering of the samples. As can be observed from Table 1, sintering is more in the case of V/CZ/T samples. Theoretical surface coverage of vanadia over the CZ/T as a function of calcination temperature is presented in Table 1.[33] As expected, the surface coverage increased with increasing calcination temperature due to sintering of the support at higher calcination temperatures.

The X-ray powder diffraction patterns of CZ/T sample calcined at various temperatures are shown in Figure 1. As can be noted from this figure, the CZ/T sample calcined at 773 K exhibits relatively poor crystallinity. In addition to the prominent TiO_2−anatase lines, few broad diffraction lines due to a mixture of Ce−Zr-oxide phases are observed. Various cubic and tetragonal Ce−Zr-oxide phases identified include $Ce_{0.75}Zr_{0.25}O_2$, $Ce_{0.6}Zr_{0.4}O_2$, $Ce_{0.5}Zr_{0.5}O_2$, and $Ce_{0.16}Zr_{0.84}O_2$. With increasing calcination temperature, the intensity of the lines pertaining to $Ce_{0.6}Zr_{0.4}O_2$ and $Ce_{0.5}Zr_{0.5}O_2$ cubic phases become more prominent, and the lines due to the cubic $Ce_{0.75}Zr_{0.25}O_2$ phase decreased. Also, the intensity of the lines pertaining to TiO_2−anatase increased because of better crystallization under the influence of thermal treatments. Recently, Preuss and Gruehn reported various Ce−Ti-oxides, Ce_2TiO_5, $Ce_2Ti_2O_7$, and $Ce_4Ti_9O_{24}$, by heating the appropriate mixtures of solids containing Ce and Ti at 1523 K.[35] However, no such crystalline phases could be seen in the present study. The TiO_2 is also known to interact with ZrO_2 to form crystalline $ZrTiO_4$ compound beyond 873 K.[36] No XRD lines pertaining to this compound are visible. The absence of crystalline $ZrTiO_4$ and Ce−Ti−O compounds may be due to a different preparation method adopted and lower calcination temperatures employed in the present investigation. It should be mentioned here that a preformed fine powder of TiO_2 was incorporated into the precipitating solutions of Ce−Zr-oxides. Therefore, the scope for the formation of compounds between titania and ceria−ziconia seems to be minimized. The deposition-precipitation technique takes advantage of the fact that precipitation onto the carrier needs a lower supersaturation than formation of new phases directly from the liquid. It is an established fact in the literature that transformation of TiO_2−anatase to rutile is thermodynamically feasible beyond 873 K in impurity-free TiO_2 samples.[33,37] However, there is no evidence regarding the formation of rutile phase even up to 1073 K in the present study. Apparently, the anatase to rutile phase transformation is somehow inhibited in the CZ/T system due to stabilization of anatase by the surrounding cerium ions as envisaged for TiO_2-SiO_2 and other mixed oxides in the literature.[38,39]

The XRD patterns of 5% V/CZ/T sample calcined at various temperatures are shown in Figure 2. The XRD patterns of the sample calcined at 773 K indicate diffraction lines due to Ce−Zr-oxides in various compositions. With increasing calcination temperature from 773 to 1073 K, the XRD lines pertaining to zirconia-rich phases become sharp and intense. In particular, the lines pertaining to the tetragonal $Ce_{0.16}Zr_{0.84}O_2$ phase become very prominent beyond 873 K. Emergence of this zirconia-rich tetragonal phase in addition to other ceria−zirconia cubic phases ($Ce_{0.6}Zr_{0.4}O_2$ and $Ce_{0.5}Zr_{0.5}O_2$) at higher calcination temperatures indicates a progressive increase of the zirconium content into the ceria lattice as a function of calcination temperature. Such a phenomenon could be regarded as surface energy driven. Because particle size is small and surface area is reasonably large (Table 1), the surface energy makes a large contribution to the total energy of the system. In this state, the cubic $Ce_{0.75}Zr_{0.25}O_2$ solid solution is thermodynamically stable at 773 K. As sintering proceeds at higher treatment temperatures and the surface area decreases, the surface energy contribution becomes smaller and demixing occurs to form more stable phases.[40,41] On the whole, the diffraction profiles of V/CZ/T samples are sharper than that of CZ/T, because of their better crystallinity, which may be due to the influence of the dispersed vanadium oxide. No XRD lines pertaining to the crystalline vanadia could be seen at all temperatures. Therefore, it can be assumed that the impregnated vanadium oxide is in a highly dispersed or amorphous state on the surface of the support. However, at 973 K and above in addition to various ceria−zirconia phases, some new lines are seen at $2\theta = 18.5$, 24, and 32.5 due to the formation of $CeVO_4$. It is an established fact in the literature that vanadium oxide interacts strongly with TiO_2, in the case of V_2O_5/TiO_2 catalysts, and forms a $V_xTi_{(1-x)}O_2$ rutile solid solution at higher calcination temperatures or during catalytic runs.[33] However, in the case of V_2O_5/TiO_2-ZrO_2 samples, a

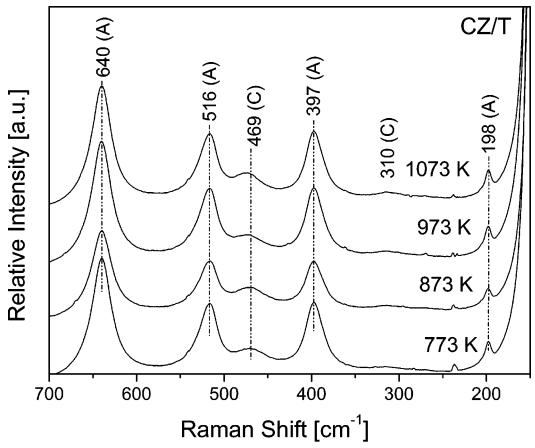

Figure 3. Raman spectra of CeO_2-ZrO_2/TiO_2 samples calcined at different temperatures.

facile formation of ZrV_2O_7 was also noted.[42] Very interestingly, the present results reveal that the formation of $CeVO_4$ is more favored than that of $V_xTi_{(1-x)}O_2$ or ZrV_2O_7 in the case of V/CZ/T samples. Ease of formation and thermal stability of vanadium oxide overlayers on various supports have been related to the ratio of charge on the support cation to the sum of radii of cation and oxide ion.[33] In general, a smaller ratio favors the compound formation. These estimations reveal that zirconia and titania have larger values than ceria, as the ionic radii of zirconium (0.84 Å) and titanium (0.64 Å) are smaller than that of cerium (0.97 Å), thus explaining the formation of stable $CeVO_4$ compound.[2,43]

The average crystallite sizes (D_{XRD}) of Ce−Zr-oxide and TiO_2 in CZ/T and V/CZ/T samples, as a function of treatment temperature, are summarized in Table 1. The full-width at half-maxima of the (111) peaks of the cubic $Zr_xCe_{1-x}O_2$ phases and (101) of the TiO_2−anatase phase were used for size calculation with the Scherrer equation. An increase in the average crystallite size of Ce−Zr-oxide is observed with increasing calcination temperature, the increase being more in the case of V/CZ/T samples. The crystallite size of TiO_2−anatase also increased with an increase in the treatment temperature. Here again, the TiO_2 crystallite size is more in the case of vanadium oxide-containing samples. Apparently, the dispersed vanadium oxide accelerates the crystallization of titania and ceria−zirconia solid solutions.[43]

The Raman spectra of CZ/T and V/CZ/T samples calcined at different temperatures are shown in Figures 3 and 4, respectively. As presented in Figure 3, the Raman spectra of CZ/T samples show typical spectra of TiO_2−anatase phase (space group $I4_1/amd$)[44] with the appearance of prominent Raman bands at 147, 196, 397, 514, and 638 cm^{-1}, which agree well with the literature reports.[45] The observed Raman band at ∼469 cm^{-1} can be attributed to the F_{2g} vibration of the fluorite type lattice. It can be viewed as a symmetric breathing mode of the oxygen atoms around cerium ions.[45] No Raman lines due to ZrO_2 are observed in line with XRD measurements. According to the literature, six Raman active modes ($A_{1g}+3E_g+2B_{1g}$) are expected for t-ZrO_2 (space group $P4_2/nmc$), while for the cubic fluorite structure of ceria (space group $Fm3m$) only one mode is Raman active.[46] As presented in Figure 3, the peak at ∼469 cm^{-1} becomes slightly intense and shifts toward higher wavenumbers with increasing calcination temperature. It should be mentioned here that the intensity of the Raman band depends on several factors including grain size and morphology.[47] It is known that sintering of samples under high-temperature conditions leads to the formation of oxygen vacancies, which perturb the local M−O bond symmetry leading to the relaxation of

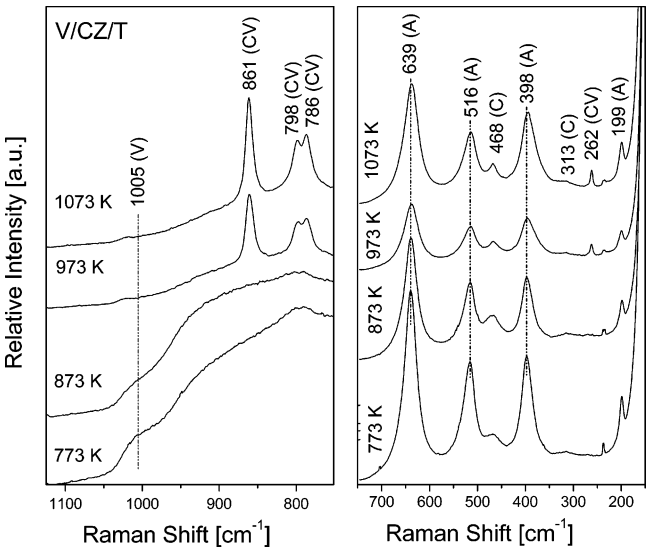

Figure 4. Raman spectra of $V_2O_5/CeO_2-ZrO_2/TiO_2$ catalysts calcined at different temperatures.

symmetry selection rules. The appearance of weak bands at ∼310 and ∼130 cm^{-1} (not shown in figure), at higher calcination temperatures, can be attributed to displacement of the oxygen atoms from their ideal fluorite lattice position.[46] It is apparent from the Raman results that ceria−zirconia support is mostly in the cubic form and does not show signs of tetragonal modification. The slight shift in the Raman frequency to higher wavenumbers could be due to an increase in the zirconia content in the ceria−zirconia solid solution as evidenced by XRD results. Thus, Raman results up to a certain extent corroborate with the XRD results, signifying the enrichment of zirconia in Ce−Zr solid solution at higher calcination temperatures.

As presented in Figure 4, the Raman spectra of V/CZ/T sample calcined at 773 K exhibit prominent peaks due to titania anatase phase and fluorite-type ceria cubic lattice along with broad and less intense bands in the region ∼945 and 995−1020 cm^{-1}. With increasing calcination temperature, the intensity of the bands pertaining to anatase and ceria cubic lattice increases proportionately, while the broad bands around 945 and 995−1020 cm^{-1} disappear progressively. At 973 K calcination temperature, few new peaks could be seen at ∼234, 262, 786, 798, and 861 cm^{-1}. These are the characteristic bands of the $CeVO_4$ phase.[48] The intensity of these bands increased with increasing calcination temperature. According to literature reports, the TiO_2−rutile phase exhibits bands at 144, 148, and 611 cm^{-1}, whose presence could not be seen in agreement with XRD results.[44] Similarly, the crystalline V_2O_5 features (Raman bands at ∼995, ∼702, ∼527, ∼404, ∼284, and ∼146 cm^{-1}) are also not apparent in line with the XRD observations.[49,50] Generally, the Raman bands of supported metal oxide catalysts in the range 1050−950 cm^{-1} are assigned to the stretching mode of the short terminal M═O bonds, whereas the bands in the range 950−750 cm^{-1} are attributed to either the antisymmetric stretch of M−O−M bonds or the symmetric stretch of $(-O-M-O-)_n$ bonds.[51,52] The presence of weak bands at ∼945 and 995−1020 cm^{-1} in the case of 773−873 K calcined samples could be assigned to the dispersed vanadia on the surface of the mixed oxide support, whose presence could not be found beyond 873 K due to $CeVO_4$ compound formation. At higher calcination temperatures, the dispersed vanadia interacts with the ceria portion of the mixed oxide leading to the formation of $CeVO_4$ stable compound. At low calcination temperatures, the impregnated vanadia is mostly in a highly dispersed state

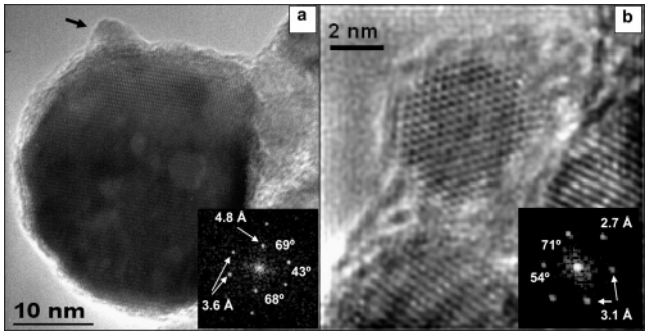

Figure 5. HREM images of CeO_2-ZrO_2/TiO_2 sample calcined at 873 K. (a) Detail of an anatase$-TiO_2$ particle. (b) Small CeO_2-ZrO_2 particle. The insets in the images are the digital diffraction patterns (DDP's) obtained from the corresponding particles.

(polyvanadate) on the surface of CZ/T. Similar findings were also reported by Bañares and Wachs for dehydrated VO_x/CeO_2 catalysts.[49,53] By employing in-situ Raman spectroscopy, they demonstrated the disappearance of surface vanadium oxide species with simultaneous formation of bulk $CeVO_4$ phase with increasing calcination temperature.[53] Raman spectroscopy is particularly powerful in the identification of the structure of amorphous systems which cannot be discerned by diffraction studies. On the whole, Raman spectra corroborate well with the XRD results.

To ascertain the results obtained from XRD and RS measurements and to explore the structural evolution at atomic scale, HREM studies were performed on some selected representative samples. The TEM images of the CZ/T sample calcined at 873 K revealed the coexistence of small crystals (∼5 nm in diameter) supported on bigger ones (∼40 nm in diameter). For deeper insight, the analyses of high-resolution images were undertaken to establish the structure and chemical composition of both types of particles. Figure 5 shows two HREM images corresponding to those two types of particles. The insets in this figure correspond to the digital diffraction patterns (DDP's) obtained from the experimental images. The different spots that are presented account for the existence of periodic contrasts in the original experimental micrographs, which correspond to different sets of atomic planes of the crystalline structure. The geometrical arrangement of these reflections is directly related to the structural aspects of the analyzed crystals. Because of this fact, the DDP's are very useful for phase recognition.[54,55] The values of 4.8 and 3.6 Å measured on the big rounded particle in Figure 5a can be respectively assigned to (002) and (101) family planes of anatase$-TiO_2$, and the geometry of the whole set of spots in the inset corresponds to the [010] zone axis of this phase. The existence of a small particle supported on top of this TiO_2 crystal has been noted as shown by a black arrow in the image. The origin of another such small particle in a different area of the sample is shown in Figure 5b. An analysis similar to that presented above, using the inset in the figure, reveals in this case the presence of *d* spacings of 3.1 and 2.7 Å. These values correspond to (111) and (002) planes of a cubic Ce$-$Zr-oxide phase, and the DDP could account for the [110] zone axis of the fluorite structure exhibited by this oxide.[56,57] From the analysis of the experimental images, the shape of the supported particles mainly exposing the more populated facets {111} and {002} is thus clearly established.

In conformity with XRD and RS analysis, the TEM image of the CZ/T sample calcined at 1073 K revealed a small increase of the particle size from 5 nm to a mean value of ∼8 nm in the case of Ce$-$Zr-oxide and no significant changes regarding the TiO_2-anatase phase. In the HREM image of the sample shown

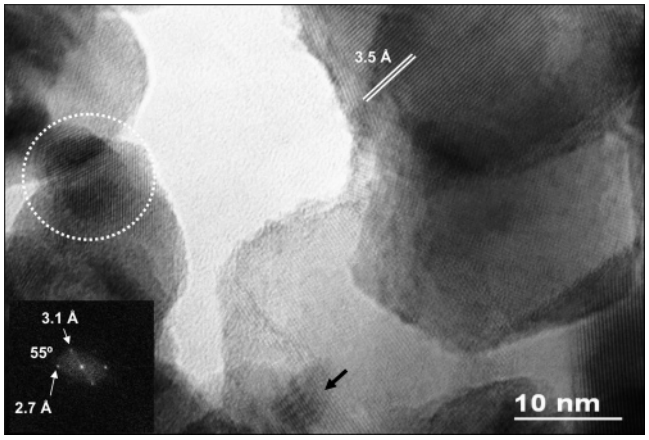

Figure 6. HREM image of CeO_2-ZrO_2/TiO_2 sample calcined at 1073 K and digital diffraction pattern corresponding to the encircled area.

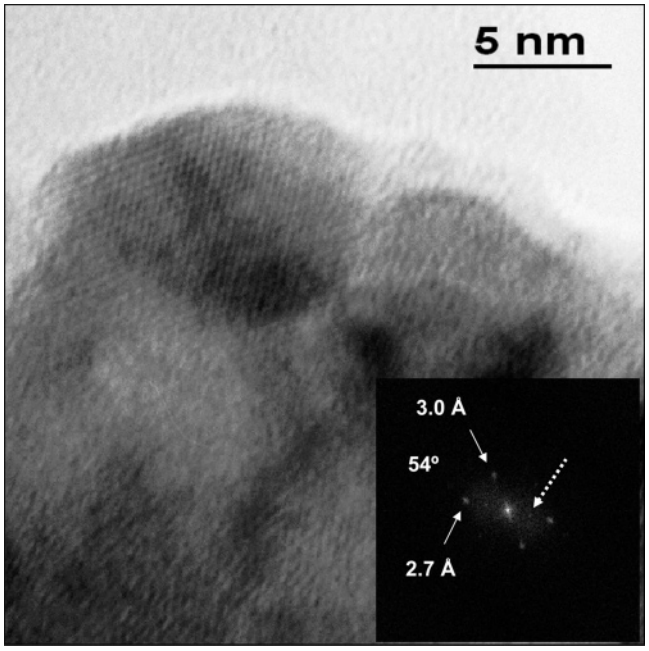

Figure 7. HREM image of CeO_2-ZrO_2/TiO_2 sample calcined at 1073 K and the digital diffraction pattern from the small supported Ce$-$Zr mixed oxide particle.

in Figure 6, the depicted *d* spacing of 3.5 Å corresponds to (101) planes of anatase structure. The complexity of this experimental image is due to the superimposed contrasts arising from different types of phases that constitute the catalyst. The existence of such mixed oxide particles is clearly affirmed by analyzing contrasts such as those encircled in Figure 6. Once again, reflections that may be assigned to (111) and (002) planes of cubic Ce$-$Zr-oxide are measured.[56] The presence of small supported particles is also revealed by moiré contrasts such as that arrowed in the figure.

As shown in Figure 7, on the basis of the analysis of DDP's calculated from some supported particles, an incorporation of more Zr atoms into the mixed oxide lattice after heating at high temperatures could be postulated. It should be noted from the inset of the figure that, in addition to the already established (111) and (002) reflections (3.1 and 2.7 Å) that correspond to the cubic phase, a new spot perfectly aligned with the latter and situated at half a distance from the center of the DDP (dot arrowed) is observed. This reflection that leads to a value of 5.4 Å could be explained if a tetragonalization of the cubic oxide is considered. The displacement of oxygen atoms introduced

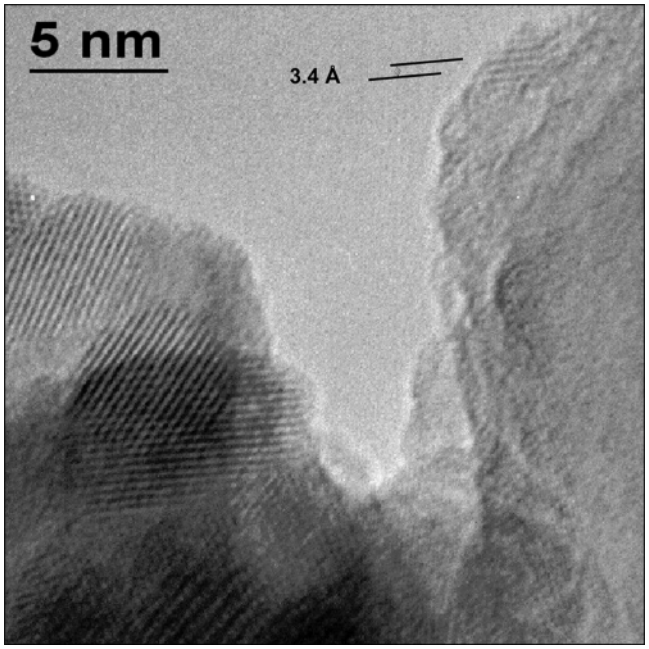

Figure 8. HREM image of $V_2O_5/CeO_2-ZrO_2/TiO_2$ sample calcined at 773 K. The periodicity of 3.4 Å corresponds to the (101) plane of V_2O_5 crystal structure.

into the structure as a consequence of Zr incorporation breaks the cubic symmetry. This fact explains the appearance of (001) periodicity (5.4 Å) which cannot be seen by XRD measurements.[56,57] These peculiar features in the experimental HREM images can be used as a guide to detect tetragonal phases in the CeO_2-ZrO_2 system.

The TEM global picture of the V/CZ/T sample calcined at 773 K revealed different types of crystals as observed in the case of vanadium-free samples. The bigger ones of ~40 nm in size could be assigned to titanium oxide crystals, and the smaller ones of ~5 nm in size due to Ce−Zr-oxide phases supported on the TiO_2 carrier were observed. Both TiO_2 crystals almost free of dispersed mixed oxide particles and others completely covered by the Ce−Zr-oxide phases were also detected. The detection of highly dispersed vanadium oxide on the mixed oxide support by TEM technique appears to be difficult, in conformity with the literature.[33] Most of the times, the dispersed vanadium oxide phase is observed in the form of small amorphous aggregates on the surface of the support,[33] which could be hardly seen if the texture of the support is so complicated as the present case. However, some contrasts observed in our experimental images have led us to identify structures that differ, in size and structural features, from that of the support (CZ/T). A representative example of this fact is shown in Figure 8. It should be noted that apart from the contrasts on the left area of the image that are similar to those previously assigned to CeO_2-ZrO_2 solid solution, a very small particle showing lattice fringes with a periodicity of 3.4 Å is detected. This measured *d* spacing could correspond to the (101) plane of V_2O_5 crystal structure. This result demonstrates a high dispersion of vanadium oxide phase on the carrier after thermal treatment at 773 K in agreement with RS results.

The TEM images of the V/CZ/T sample calcined at 1073 K revealed the presence of two types of crystals, the bigger ones corresponding to TiO_2 and relatively smaller ones over the bigger crystals due to the Ce−Zr-oxides. The HREM images and the corresponding DDP's of the smaller particles due to Ce−Zr-oxides revealed the coexistence of zirconium-rich and cerium-rich phases. Further, the crystallite size of Ce−Zr-oxides

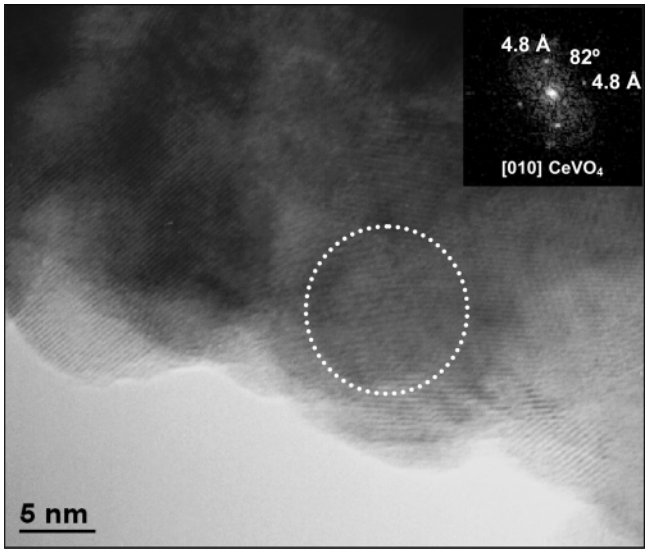

Figure 9. HREM image of $V_2O_5/CeO_2-ZrO_2/TiO_2$ sample calcined at 1073 K and the digital diffraction pattern of the encircled area of the image.

was grown proportionately with respect to the particles observed in the case of CZ/T support and V/CZ/T (773 K) sample, indicating that the presence of dispersed vanadium oxide favors both sintering of the Ce−Zr-oxide phases and their partial enrichment with zirconium. Evidence for a chemical interaction between the dispersed vanadium oxide and the cerium-rich phases is presented in Figure 9. The DDP obtained from the encircled area in the image clearly reveals the existence of two spots at a value of 4.8 Å and an angle of 82° between them. These features match quite well with the characteristics of the [010] zone axis of the $CeVO_4$ phase, where the measured *d* spacing accounts for the (101) planes of the vanadate structure. Periodicities of 3.7 Å taken in different areas of the sample, which could correspond to (200) planes of cerium vanadate, confirm the detection of such structure. Thus, the TEM results corroborate well with the observations made from XRD and RS measurements. Thus, the combined XRD, RS, and HREM studies provided valuable information on the structural evolution of CZ/T and V/CZ/T mixed oxide catalysts. The oxygen storage characteristics (OSC) of these materials and the catalytic properties for preferential oxidation of CO and other nonselective oxidations have been evaluated, and the preliminary results are found to be highly encouraging. Further studies are under active progress.

Conclusions

By adopting the deposition precipitation methodology, the preparation of 1:1:2 mole ratio CeO_2-ZrO_2/TiO_2 was undertaken. Further, a nominal 5 wt % V_2O_5 was impregnated over the surface of the mixed oxide. This preparation yields fairly homogeneous and well-dispersed Ce−Zr-oxides over the TiO_2 surface. (2) The influence of thermal treatments from 773 to 1073 K on the deposited oxide components was examined using XRD, Raman, and HREM techniques. Better crystallization of various Ce−Zr mixed oxides was observed with increasing treatment temperature. (3) The CZ/T sample calcined at lower temperatures exhibited relatively small crystallites (~5 nm) of dispersed Ce−Zr-oxides over the surface of bigger crystals (~40 nm) of TiO_2. (4) The XRD results revealed the formation of $Ce_{0.75}Zr_{0.25}O_2$, $Ce_{0.6}Zr_{0.4}O_2$, $Ce_{0.5}Zr_{0.5}O_2$, and $Ce_{0.16}Zr_{0.84}O_2$ phases in varying proportions depending on the treatment

temperature. (5) Impregnation of V_2O_5 on the surface of CZ/T showed a strong influence on the Ce−Zr mixed oxide phases and their crystallite size. A better crystallization and more incorporation of zirconia into the ceria lattice were noted. In particular, the formation of $CeVO_4$ and an intense tetragonal $Ce_{0.16}Zr_{0.84}O_2$ phase was observed beyond 873 K. (6) The TiO_2 was mainly in anatase form irrespective of treatment temperature and the presence or absence of vanadium oxide as revealed by all characterization techniques employed. The characterization results further suggest that the formation of $CeVO_4$ is more favored than that of the $V_xTi_{(1-x)}O_2$ or ZrV_2O_7 in the case of V/CZ/T samples.

Acknowledgment. We thank Dr. S. Loridant, Institut de Recherches sur la Catalyse-CNRS, Villeurbanne, France, for helpful suggestions on Raman results. A.K. and P.L. thank CSIR, New Delhi, for Senior and Junior Research Fellowships, respectively. C.L.-C. thanks the I3P program (CSIC) for a postdoctoral contract.

References and Notes

(1) Gandhi, H. S.; Graham, G. W.; McCabe, R. W. *J. Catal.* **2003**, *216*, 433 and references therein.
(2) Trovarelli, A.; de Leitenburg, C.; Dolcetti, G. *CHEMTECH* **1997**, *27*, 32.
(3) Bernal, S., Kaspar, J., Trovarelli, A., Eds. Recent Progress in Catalysis by Ceria and Related Compounds. *Catal. Today* **1999**, *50*, 173.
(4) Nelson, A. E.; Schulz, K. H. *Appl. Surf. Sci*. **2003**, *210*, 206.
(5) Daturi, M.; Finocchio, E.; Binet, C.; Lavalley, J. C.; Fally, F.; Perrichon, V. *J. Phys. Chem. B* **1999**, *103*, 4884.
(6) Pijolat, M.; Prin, M.; Soustelle, M.; Touret, O.; Nortier, P. *J. Chem. Soc., Faraday. Trans*. **1995**, *91*, 3941.
(7) Kozlov, A.; Kim, D. H.; Yezerets, A.; Anderson, P.; Kung, H. H.; Kung, M. F. *J. Catal.* **2002**, *209*, 417.
(8) Sugiura, M. *Catal. Surv. Jpn.* **2003**, *7*, 77.
(9) Hori, C. E.; Permana, H.; Ng, K. Y. S.; Brenner, A.; More, K.; Rahmoeller, K. M.; Belton, D. *Appl. Catal., B* **1998**, *16*, 105.
(10) Lemaux, S.; Bensaddik, A.; Van der Eerden, A. M. J.; Bitter, J. H.; Koningsberger, D. C. *J. Phys. Chem. B* **2001**, *105*, 4810.
(11) Sahibzada, M.; Steele, B. C. H.; Zheng, K.; Rudkin, R. A.; Metcalfe, I. S. *Catal. Today* **1997**, *38*, 459.
(12) Larachi, F.; Pierre, J.; Adnot, A.; Bernis, A. *Appl. Surf. Sci*. **2002**, *195*, 236.
(13) Qi, G.; Yang, R. T. *Chem. Commun*. **2003**, 848.
(14) Centeno, M. A.; Paulis, M.; Montes, M.; Odriozola, J. A. *Appl. Catal., A* **2002**, *234*, 65.
(15) Zamar, F.; Trovarelli, A.; de Leitenburg, C.; Dolcetti, G. *J. Chem. Soc., Chem. Commun.* **1995**, 965.
(16) Nagai, Y.; Yamamoto, T.; Tanaka, T.; Yoshida, S.; Nonaka, T.; Okamoto, T.; Suda, A.; Sugiura, M. *Catal. Today* **2002**, *74*, 225.
(17) Chen, K.; Khodakov, A.; Yang, J.; Bell, A. T.; Iglesia, E. *J. Catal.* **1999**, *186*, 325.
(18) Concepción, P.; López-Nieto, J. M.; Pérez-Pariente, J. *J. Mol. Catal. A* **1995**, *99*, 173.
(19) Weckhuysen, B. M.; Wang, D.; Rosynek, M. P.; Lunsford, J. H. *J. Catal.* **1998**, *175*, 347.
(20) Bosch, H.; Janssen, F. *Catal. Today* **1988**, *2*, 369.
(21) Amiridis, M. D.; Wachs, I. E.; Deo, G.; Jehng, J. M.; Kim, D. S. *J. Catal.* **1996**, *161*, 247.
(22) Concepción, P.; Reddy, B. M.; Knözinger, H. *Phys. Chem. Chem. Phys.* **1999**, *1*, 3031.
(23) Cavelli, P.; Cavani, I.; Manenti, I.; Trifiro, F. *Catal. Today* **1987**, *1*, 245.
(24) Reddy, B. M.; Kumar, M. V.; Ratnam, K. J. *Appl. Catal., A* **1999**, *181*, 77.
(25) Daniell, W.; Ponchel, A.; Kuba, S.; Anderle, F.; Weingand, T.; Gregory, D. H.; Knözinger, H. *Top. Catal*. **2002**, *20*, 65.
(26) Rane, V. H.; Rajput, A. M.; Karkamkar, A. J.; Choudhary, V. R. *Appl. Energy* **2004**, *77*, 375.
(27) Feng T.; Vohs, J. M. *J. Catal.* **2004**, *221*, 619.
(28) Burcham, L. J.; Deo, G.; Gao, X.; Wachs, I. E. *Top. Catal*. **2000**, *11/12*, 85.
(29) Martinez-Huerta, M. V.; Coronado, J. M.; Fernandez-Garcia, M.; Iglesias-Juez, A.; Deo, G.; Fierro, J. L. G.; Banares, M. A. *J. Catal*. **2004**, *225*, 240.
(30) Wootsch, A.; Descorme, C.; Duprez, D. *J. Catal*. **2004**, *225*, 259.
(31) Reddy, B. M. Redox Properties of Metal Oxides. In *Metal Oxides: Chemistry and Applications*; Fierro, J. L. G., Ed.; Marcel Dekker Inc., In press.
(32) Klug, H. P.; Alexander, L. E. *X-ray Diffraction Procedures for Polycrystalline and amorphous materials*, 2nd ed.; John Wiley and Sons: New York, 1974.
(33) Bond, G. C.; Tahir, S. F. *Appl. Catal.* **1991**, *71*, 1 and references therein.
(34) Reddy, B. M.; Ganesh, I.; Reddy, E. P. *J. Phys. Chem. B* **1997**, *101*, 1769.
(35) Preuss, A.; Gruehn, R. *J. Solid State Chem*. **1994**, *110*, 363.
(36) Reddy, B. M.; Manohar, B.; Mehdi, S. *J. Solid State Chem*. **1992**, *97*, 233.
(37) Hadjiivanov, K. I.; Klissurski, D. G. *Chem. Soc. Rev.* **1996**, *25*, 61.
(38) Lin, J.; Yu, J. C. *J. Photochem. Photobiol., A* **1998**, *116*, 63.
(39) Anderson, C.; Bard, A. J. *J. Phys. Chem.* **1994**, *98*, 1769.
(40) Kenevey, K.; Valdivieso, F.; Soustelle, M.; Pijolat, M. *Appl. Catal., B* **2001**, *29*, 93.
(41) Reddy, B. M.; Khan, A.; Yamada, Y.; Kobayashi, T.; Loridant, S.; Volta, J. C. *Langmuir* **2003**, *19*, 3025.
(42) Reddy, B. M.; Chowdhary, B.; Ganesh, I.; Reddy, E. P.; Rojas, T. C.; Fernández, A. *J. Phys. Chem. B* **1998**, *102*, 10176.
(43) Reddy, B. M.; Khan, A.; Yamada, Y.; Kobayashi, T.; Loridant, S.; Volta, J. C. *J. Phys. Chem. B* **2003**, *107*, 11475.
(44) Kosmulski, M. *Adv. Colloid Interface Sci.* **2002**, *99*, 255.
(45) Lin, X.-M.; Li, L.-P.; Li, G.-S.; Su, W.-H. *Mater. Chem. Phys*. **2001**, *69*, 236.
(46) Yashima, M.; Arashi, H.; Kakihana, M.; Yoshimura, M. *J. Am. Ceram. Soc.* **1994**, *77*, 1067.
(47) Spanier, J. E.; Robinson, R. D.; Zhang, F.; Chan, S.-W.; Herman, I. P. *Phys. Rev. B* **2001**, *64*, 245407.
(48) Hirata, T.; Watanabe, A. *J. Solid State Chem*. **2001**, *158*, 254.
(49) Bañares, M. A.; Wachs, I. E. *J. Raman Spectrosc.* **2002**, *33*, 359.
(50) Olthof, B.; Khodakov, A.; Bell, A. T.; Iglesia, E. *J. Phys. Chem. B* **2000**, *104*, 1516.
(51) Knözinger, H.; Mestl, G. *Top. Catal*. **1999**, *8*, 45.
(52) Wachs, I. E. *Top. Catal*. **1999**, *8*, 57.
(53) Bañares, M. A.; Martinez-Huerta, M. V.; Gao, X.; Fierro, J. L. G.; Wachs, I. E. *Catal. Today* **2000**, *61*, 295.
(54) Bernal, S.; Baker, R. T.; Burrows, A.; Calvino, J. J.; Kiely, C. J.; López-Cartes, C.; Pérez-Omil, J. A.; Rodríguez-Izquierdo, J. M. *Surf. Interface Anal.* **2000**, *29*, 411.
(55) Bernal, S.; Calvino, J. J.; Cauqui, M. A.; Gatica, J. M.; Lopez-Cartes, C.; Perez-Omil, J. A.; Pintado, J. M. *Catal. Today* **2003**, *77*, 385.
(56) Colon, G.; Pijolat, M.; Valdivieso, F.; Vidal, H.; Kaspar, J.; Finocchio, E.; Daturi, M.; Binet, C.; Lavalley, J. C.; Baker, R. T.; Bernal, S. *J. Chem. Soc., Faraday Trans*. **1998**, *94*, 3717.
(57) Colon, G.; Valdivieso, F.; Pijolat, M.; Baker, R. T.; Calvino, J. J.; Bernal, S. *Catal. Today* **1999**, *50*, 271.